PTF 10bzf (SN 2010ah): a broad-line Ic supernova discovered by the Palomar Transient Factory

A. Corsi[1], E. O. Ofek[2,3], D. A. Frail[4], D. Poznanski[3,5,6], I. Arcavi[7] , A. Gal-Yam[7], S. R. Kulkarni[2], K. Hurley[8], P. A. Mazzali[9,10], D. A. Howell[11,12], M. M. Kasliwal[2], Y. Green[7], D. Murray[11,12], M. Sullivan[13], D. Xu[7], S. Ben-ami[7], J. S. Bloom[6], S. B. Cenko[6], N. M. Law[14], P. Nugent[5,6], R. M. Quimby[2], V. Pal'shin[15], J. Cummings[16], V. Connaughton[17], K. Yamaoka[18], A. Rau[19], W. Boynton[20], I. Mitrofanov[21], J. Goldsten[22]

ABSTRACT

[1]LIGO laboratory, California Institute of Technology, MS 100-36, Pasadena, CA 91125, USA;

corsi@caltech.edu

[2]Cahill Center for Astrophysics, California Institute of Technology, Pasadena, CA, 91125, USA

[3]Einstein Fellow

[4]National Radio Astronomy Observatory, P.O. Box 0, Socorro, NM 87801, USA

[5]Computational Cosmology Center, Lawrence Berkeley National Laboratory, 1 Cyclotron Road, Berkeley, CA 94720, USA

[6]Department of Astronomy, 601 Campbell Hall, University of California, Berkeley, CA 94720-3411, USA

[7]Department of Particle Physics and Astrophysics, The Weizmann Institute of Science, Rehovot 76100, Israel

[8]Space Sciences Laboratory, University of California Berkeley, 7 Gauss Way, Berkeley, CA 94720, USA

[9]INAF - Osservatorio Astronomico, vicolo dell'Osservatorio, 5, I-35122 Padova, Italy

[10]Max-Planck Institut für Astrophysik, Karl-Schwarzschildstr. 1, D-85748 Garching, Germany

[11]Las Cumbres Observatory Global Telescope Network, Inc, Santa Barbara, CA, 93117, USA

[12]Department of Physics, University of California Santa Barbara, Santa Barbara, CA 93106, USA

[13]Department of Physics (Astrophysics), University of Oxford, DWB, Keble Road, Oxford, OX1 3RH, UK

[14]Dunlap Institute for Astronomy and Astrophysics, University of Toronto, 50 St. George Street, Toronto M5S 3H4, Ontario, Canada

[15]Ioffe Physico-Technical Institute of the Russian Academy of Sciences, St. Petersburg, Russian Federation

[16]University of Maryland, Baltimore County (UMBC), 1000 Hilltop Circle, Baltimore, MD 21250

[17]University of Alabama in Huntsville CSPAR, Huntsville AL

[18]Department of Physics and Mathematics, Aoyama Gakuin University, Kanagawa, Japan

[19]Max-Planck-Institut für extraterrestrische Physik, Garching, Germany

[20]University of Arizona, Department of Planetary Sciences, Tucson, AZ

[21]Space Research Institute, Moscow, Russian Federation

[22]Applied Physics Laboratory, Johns Hopkins University, Laurel, MD

We present the discovery and follow-up observations of a broad-line type-Ic supernova (SN), PTF 10bzf (SN 2010ah), detected by the Palomar Transient Factory (PTF) on 2010 February 23. The SN distance is $\cong$ 218 Mpc, greater than GRB 980425 / SN 1998bw and GRB 060218 / SN 2006aj, but smaller than the other SNe firmly associated with gamma-ray bursts (GRBs). We conducted a multi-wavelength follow-up campaign with Palomar-48 inch, Palomar 60-inch, Gemini-N, Keck, Wise, *Swift*, the Allen Telescope Array, CARMA, WSRT, and EVLA. Here we compare the properties of PTF 10bzf with those of SN 1998bw and other broad-line SNe. The optical luminosity and spectral properties of PTF 10bzf suggest that this SN is intermediate, in kinetic energy and amount of ^{56}Ni, between non GRB-associated SNe like 2002ap or 1997ef, and GRB-associated SNe like 1998bw. No X-ray or radio counterpart to PTF 10bzf was detected. X-ray upper-limits allow us to exclude the presence of an underlying X-ray afterglow as luminous as that of other SN-associated GRBs like GRB 030329 or GRB 031203. Early-time radio upper-limits do not show evidence for mildly-relativistic ejecta. Late-time radio upper-limits rule out the presence of an underlying off-axis GRB, with energy and wind density similar to the SN-associated GRB 030329 and GRB 031203. Finally, by performing a search for a GRB in the time window and at the position of PTF 10bzf, we find that no GRB in the IPN catalog could be associated with this SN.

Subject headings: supernovae: general — supernovae: individual (PTF 10bzf) — Gamma-ray: general — radiation mechanisms: non-thermal

1. Introduction

The Palomar Transient Factory[1] (PTF; Law et al. 2009; Rau et al. 2009) is an on-going project optimized for detecting optical transients in the local Universe. One of its main objectives is the collection of a large sample of core-collapse supernovae (SNe; e.g. Arcavi et al. 2010), for which multicolor optical light-curves and spectra can be obtained through dedicated follow-up resources.

The explosive death of a SN massive progenitor occurs when its iron core collapses to a neutron star or a black hole. Core-collapse SNe are either of type Ib/Ic if the Hydrogen envelope of the progenitor is lost, or else of Type II (Filippenko 1997). While the total kinetic energy released in the explosion is of the order of 10^{51} erg, roughly the same as the energy of the jet that makes a gamma-ray burst (GRB), core-collapse SNe are in general not accompanied by highly relativistic mass ejection, and are visible from all angles.

The discovery of an association between a Ic SN and a long duration GRB in 1998 (Galama et al. 1998; Kulkarni et al. 1998), strongly supported the collapsar scenario (e.g. MacFadyen & Woosley 1999a; Mészáros 2006; Woosley & Bloom 2006, and references therein). This was one of the most unusual Type Ic SNe seen up to that time: more luminous than typical Ic SNe, with broad lines and strong radio emission indicating a relativistic expansion speed ($\Gamma \sim 2$; Kulkarni et al. 1998).

---

[1]http://www.astro.caltech.edu/ptf/

Since 1998, a total of five associations between GRBs and SNe have been spectroscopically confirmed (Table 1). GRBs with spectroscopically confirmed SNe are generally under-luminous and sub-energetic in comparison to typical long GRBs. A notable exception, though, is GRB 030329 associated with SN 2003dh, that represents the first solid evidence for a connection between ordinary GRBs and SNe (Garnavich et al. 2003; Hjorth et al. 2003; Kawabata et al. 2003; Matheson et al. 2003; Stanek et al. 2003).

After GRB 030329, a SN-like brightening was reported at the position of GRB 031203, and SN 2003lw was then photometrically (Bersier et al. 2004; Cobb et al. 2004; Malesani et al. 2004; Gal-Yam et al. 2004), and spectroscopically (Malesani et al. 2004) confirmed to be associated with this GRB. Broad spectral features similar to SN 1998bw also characterized SN 2003lw.

The understanding of the GRB-SN connection has further progressed thanks to discovery of GRB/XRF 060218 (Pian et al. 2006; Modjaz et al. 2006; Sollerman et al. 2006; Ferrero et al. 2006), associated with SN 2006aj. The prompt spectrum of this GRB showed evidence for a typical non-thermal component (as observed also in ordinary GRBs), plus a thermal component. This last suggested that the shock breakout of an associated SN was for the first time being observed (Campana et al. 2006; Waxman et al. 2007). A different central engine (a magnetar rather than a black hole), was also suggested by several authors to explain the long-duration and lower luminosity of GRB 060218 (Mazzali et al. 2006b; Soderberg et al. 2006b; Toma et al. 2007).

The breakout of a shock through the stellar surface is predicted to be the first electromagnetic signal marking the birth of a SN. The typical frequency of the emission is in the soft γ-rays for core-collapse SNe (Grassberg et al. 1971; Chevalier 1976, 1992; Waxman et al. 2007; Chevalier & Fransson 2008; Katz et al. 2010; Nakar & Sari 2010; Balberg & Loeb 2011; Katz et al. 2011; Nagakura et al. 2011; Rabinak & Waxman 2011). Since XRF 060218, several shock breakout candidate events have been proposed (Soderberg et al. 2008; Gezari et al. 2008; Schawinski et al. 2008; Modjaz et al. 2009; Ofek et al. 2010b). Multi-wavelength observations of core-collapse SN are fundamental to probe the breakout phase.

The most recent spectroscopically confirmed association between a GRB and a SN is represented by the case of GRB 100316D (Starling et al. 2010) and SN 2010bh (Bufano et al. 2010; Chornock et al. 2010; Wiersema et al. 2010; Cano et al. 2011). GRB 100316D was a long-duration, soft-spectrum GRB, resembling GRB 060218 in these properties.

While the above mentioned observations have clearly established a connection between long-duration GRBs and type Ic core-collapse SNe, however, what makes some broad-line Ic SNe have an accompanying GRB is still a mystery. Some long GRBs are clearly not associated with a SN, e.g. GRB 060505 (Ofek et al. 2007) and GRB 060614 (Della Valle et al. 2006; Fynbo et al. 2006; Gal-Yam et al. 2006a). On the other hand, SN 1997ef remains so far the most energetic peculiar Ic SN without a clear GRB association (e.g. Mazzali et al. 2000), and the broad-line Ic SN 2009bb (Soderberg et al. 2010) showed clear evidence of very high expansion velocity (as normally seen in GRB-related SNe), but no clear GRB association. However, it is remarkable that all GRB-related SNe discovered to date are broad line Ic SNe.

Theoretically, in order to produce a relativistic jet from a collapsing star to power the observed GRB, the stellar core has to carry a high angular momentum (Woosley & Heger 2006), so that the spin axis provides a

natural preferred propagation direction for the jet. Moreover, the jet needs to be "clean", with small baryon contamination, so that it can achieve a relativistic speed, with Lorentz factor Γ typically greater than 100 (Piran 1999; Lithwick & Sari 2001; Liang et al. 2010; Abdo et al. 2009b,a,c; Corsi et al. 2010). The outflow also needs to be collimated, with an aperture angle of the order of $1° - 10°$ for bright GRBs (Frail et al. 2001; Bloom et al. 2003; Liang et al. 2008; Racusin et al. 2009).

Several types of GRB central engine have been discussed, the leading candidate being a black hole plus torus system (Woosley 1993; MacFadyen & Woosley 1999b; Proga & Begelman 2003; Zhang et al. 2003). An alternative candidate is a rapidly spinning, highly magnetized neutron star (magnetar, e.g. Usov 1992; Thompson et al. 2004; Bucciantini et al. 2008; Metzger et al. 2011). In the black hole scenario, the first energy source is the accretion power from the torus. On the other hand, the main power of a millisecond magnetar engine is its spin down power.

Whatever the nature of the GRB central engine is, it has to generate both a narrowly collimated, highly relativistic jet to make the GRB, and a wide angle, sub-relativistic outflow responsible for exploding the star and making the SN. To some extent, the two components may vary independently, so it is possible to produce a variety of jet energies and SN luminosities. Woosley & Zhang (2007) have shown that at least a $\sim 10^{48}$ erg s^{-1} power is required for a jet to escape a massive star before that star either explodes or is accreted, and lower energy and "suffocated" bursts may be particularly prevalent when the metallicity is high, i.e., in the modern universe at low redshift.

A key prediction of jet models for GRBs (e.g. Piran 2004), combined with the association of long GRBs with type Ib/Ic core-collapse SNe (e.g. Woosley & Bloom 2006), is that some (spherical) SN explosions will be accompanied by off-axis GRBs, whose gamma-ray signal is missed because the jet is not pointed at us, but whose afterglow emission could be visible at lower energies (from radio to X-rays), once the jet decelerates. These are also referred to as "orphan afterglows". Detecting an off-axis GRB would constitute a direct proof of the popular jet model for GRBs but, after a decade of efforts (Berger et al. 2003b; Gal-Yam et al. 2006b; Soderberg et al. 2006b), such a detection has not yet been achieved. Orphan afterglows may also be produced by "dirty fireballs", i.e., cosmological fireballs whose ejecta carry too many baryons to produce a GRB. Multi-color, wide-area searches, combined with radio follow-up, can help distinguishing between off-axis GRBs and dirty fireballs (Perna & Loeb 1998; Rhoads 2003).

Based on radio follow-up campaigns of Ib/c SNe (Berger et al. 2003b; Soderberg et al. 2010), it is now believed that no more than 1% of SNe type Ib/c are powered by central engines. These observational facts are giving us hints at the fundamental role that broad-line Ic SNe play in engine-drive explosions. GRBs are known to prefer low-metallicity dwarf galaxies (e.g. Fynbo et al. 2003; Fruchter et al. 2006), and to be associated only with a particular subclass of core-collapse SNe: broad-line Ic events. Previous searches, however, targeted mostly regular SNe Ib/Ic, residing in giant, high-metallicity hosts. This is why broad-line Ic events deserve to be studied with particular attention (Modjaz et al. 2008).

Multi-wavelength follow-up campaigns of broad-line Ib/c SNe are especially important to probe high expansion velocities, and/or any associated GRB. Moreover, because of their low (electromagnetic) luminosity compared to GRBs, usually SNe are observed at non-cosmological distances ($z \lesssim 1$). Thus, broad-line

Ib/c also represent a tool to search for nearby GRB explosions and understand their connection with cosmological GRBs (e.g. Norris 2002; Podsiadlowski et al. 2004; Guetta & Della Valle 2007; Liang et al. 2007; Virgili et al. 2009).

In this paper, we present the discovery of a broad-line Ic SN, PTF 10bzf (SN 2010ah), detected by PTF. This event is interesting because of two reasons. First, as a broad-line SN located at a distance smaller than most GRB-associated events (except for GRB 980425 / SN 1998bw and GRB 060218 / SN 2006aj, see Table 1). Next, this event enjoyed a rich radio-to-X-ray follow-up campaign. In what follows, we first describe the observations that led to the discovery of PTF 10bzf (§2), and its multi-wavelength follow-up campaign (§3). Then, we compare PTF 10bzf with SN 1998bw and other GRB-associated SNe, and describe the results of an associated GRB search (§4). Finally, we conclude in §5.

2. Observations and data reduction

On 2010 February 23.5038 (hereafter all times are given in UTC), we discovered a broad-line type-Ic SN, PTF 10bzf, visible at a magnitude of $R \approx 18.86$ (see Table 2 and Figure 1), in a 60 s exposure image taken with the Palomar 48-inch telescope (P48). The SN was not seen in previous images of the same field taken on 2010 February 19.4392, down to a limiting magnitude of $R > 21.3$. The SN J2000 position is RA=11:44:02.99, Dec=+55:41:27.6 (Ofek et al. 2010a), $\cong 5''.2$ offset, and at a position angle of $\cong 5 \deg$ (North through East) about the position of the galaxy SDSS[2] J114402.98+554122.5.

Digital copies of our data can be downloaded directly from the Weizmann Institute of Science Experimental Astrophysics Spectroscopy System (WISEASS[3], Yaron et al. 2011).

2.1. Optical photometry

P48 observations of the PTF 10bzf field were performed with the Mould-R filter. A high-quality image produced by stacking several images of the same field (obtained between May 2009 and June 2009), was used as a reference and subtracted from the individual images. Photometry was performed relative to the r-band magnitudes of ten SDSS reference stars in the field, including r-i color term corrections, using an aperture of 2 arc sec radius, and applying aperture corrections to account for systematic errors and errors introduced by the subtraction process. Aperture corrections are all below ≈ 0.04 mag. All the P48 photometry is listed in Table 2. The P48 calibrated light-curve of PTF 10bzf is plotted in Figure 2.

P60 observations were carried out in the B, g, r, i, z bands. We also observed the PTF 10bzf field

---

[2]Sloan Digital Sky Survey (York et al. 2000).

[3]http://www.weizmann.ac.il/astrophysics/wiseass/

Table 1. Summary of light-curve properties

SN	type	Associated GRB	$d_{\rm L}$ Mpc	$M_{\rm R}$ (mag)	$M_{Ni}/M_\odot$
SN 1998bw[a]	engine-driven BL-Ic	GRB 980425	37	-19.36 ± 0.05	$0.4 - 0.5$
SN 2003dh[b]	engine-driven BL-Ic	GRB 030329	810	≈ -19	$0.25 - 0.45$
SN 2003lw[c]	engine-driven BL-Ic	GRB 031203	477	-19.90 ± 0.08	$0.45 - 0.65$
SN 2006aj[d]	engine-driven BL-Ic	GRB 060218	140	-18.81 ± 0.06	0.21
SN 2010bh[e]	engine-driven BL-Ic	GRB 100316D	261	-	-
SN 2009bb[f]	engine-driven BL-Ic	none	40	-18.56 ± 0.28	0.16-0.28
SN 2003jd[g]	BL-Ic	none	78	-18.94 ± 0.30	0.26-0.45
SN 2002ap[h]	BL-Ic	none	7.8	-17.50 ± 0.32	0.06-0.12

Note. — See also Woosley & Bloom (2006), and references therein, for a recent review.

[a]Galama et al. (1998); Iwamoto et al. (1998); Nakamura et al. (2001)

[b]Hjorth et al. (2003); Matheson et al. (2003); Deng et al. (2005)

[c]Malesani et al. (2004); Mazzali et al. (2006b)

[d]Mazzali et al. (2006a); Pian et al. (2006); Soderberg et al. (2006b); Valenti et al. (2008)

[e]Starling et al. (2010)

[f]Pignata et al. (2011)

[g]Mazzali et al. (2005); Valenti et al. (2008); Drout et al. (2010)

[h]Gal-Yam et al. (2002); Mazzali et al. (2002); Foley et al. (2003); Drout et al. (2010)

with the 1 m telescope at the Wise observatory[4] using *BVRI* filters (see Table 2). For both P60 and Wise observations, image subtraction was performed using the common point spread function method via the "mkdifflc" routine (Gal-Yam et al. 2004, 2008). Errors on the P60 and Wise data are estimated by using "artificial" sources at a brightness similar to that of the real SN, with the scatter in their magnitudes providing an estimate of the error due to subtraction residuals. The measured magnitude was calibrated against the magnitudes of SDSS stars in the same field (see Figure 1). The calibration procedure described in Jordi et al. (2006) was used for the *BVRI* data. Calibration errors were summed in quadrature with the subtraction errors.

---

[4]http://wise−obs.tau.ac.il/

Table 2.   PTF 10bzf follow-up campaign.

| JD-2455251.004 (days since Feb 23.504)	Telescope	Δt (s)	Band	Mag or Flux	Reference
-4.061	P48	60	Mould-R	> 21.3	ATEL 2470
0.000	P48	60	Mould-R	18.863 ± 0.041	ATEL 2470
0.045	P48	60	Mould-R	18.850 ± 0.056	This paper
18.038	P48	60	Mould-R	18.362 ± 0.040	This paper
18.921	P48	60	Mould-R	18.527 ± 0.030	This paper
18.966	P48	60	Mould-R	18.495 ± 0.030	This paper
21.832	P48	60	Mould-R	18.599 ± 0.036	This paper
21.876	P48	60	Mould-R	18.618 ± 0.039	This paper
24.866	P48	60	Mould-R	18.791 ± 0.033	This paper
24.911	P48	60	Mould-R	18.735 ± 0.034	This paper
28.727	P48	60	Mould-R	18.966 ± 0.062	This paper
28.771	P48	60	Mould-R	18.861 ± 0.042	This paper
31.636	P48	60	Mould-R	19.12 ± 0.11	This paper
31.679	P48	60	Mould-R	19.061 ± 0.085	This paper
33.650	P48	60	Mould-R	19.18 ± 0.11	This paper
33.693	P48	60	Mould-R	19.093 ± 0.081	This paper
38.758	P48	60	Mould-R	19.381 ± 0.050	This paper
38.802	P48	60	Mould-R	19.359 ± 0.053	This paper
39.857	P48	60	Mould-R	19.393 ± 0.058	This paper
39.901	P48	60	Mould-R	19.401 ± 0.057	This paper
42.670	P48	60	Mould-R	19.547 ± 0.062	This paper
42.713	P48	60	Mould-R	19.480 ± 0.065	This paper
43.829	P48	60	Mould-R	19.576 ± 0.061	This paper
43.873	P48	60	Mould-R	19.723 ± 0.065	This paper
44.926	P48	60	Mould-R	19.597 ± 0.053	This paper
44.962	P48	60	Mould-R	19.531 ± 0.059	This paper
45.983	P48	60	Mould-R	19.696 ± 0.067	This paper
45.984	P48	60	Mould-R	19.764 ± 0.075	This paper
60.737	P48	60	Mould-R	19.800 ± 0.093	This paper
60.781	P48	60	Mould-R	19.89 ± 0.11	This paper
61.783	P48	60	Mould-R	19.96 ± 0.12	This paper
61.826	P48	60	Mould-R	20.23 ± 0.13	This paper
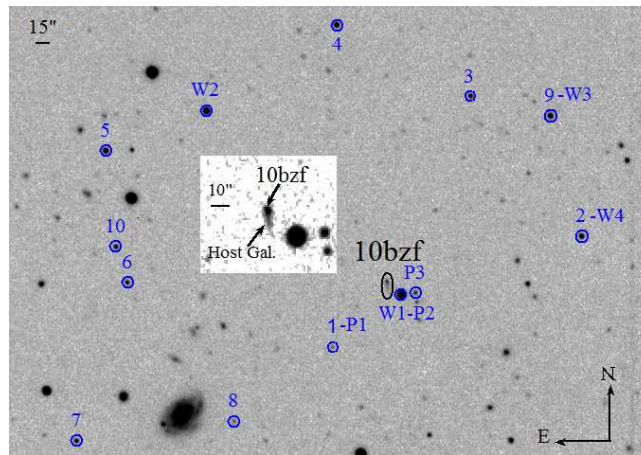
Fig. 1.— P48 discovery image of PTF 10bzf in the *R*-band. For clarity purposes, a circle of 5″ radius marks the position of the ten reference stars used for P48 photometry calibration (1-10), and of the four reference stars used for calibration of the Wise data (W1-W4). The stars labeled as P1-P3 were used for the calibration of P60 photometry. The position of PTF 10bzf and its host galaxy are enclosed by a black ellipse. The inset shows in more detail PTF 10bzf inside its host. The SN is located at RA=11:44:02.99 and Dec=+55:41:27.6 (J2000).
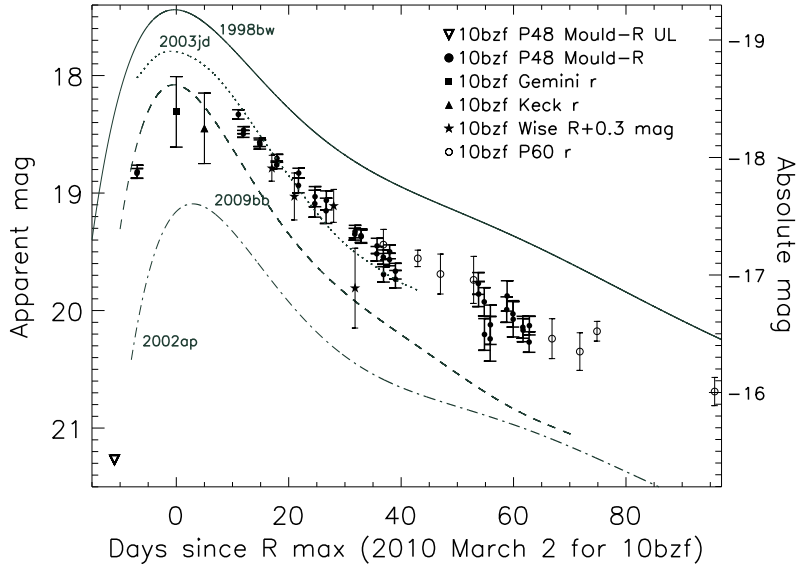
Fig. 2.— Light-curve of PTF 10bzf corrected for Galactic extinction. Absolute magnitudes are plotted on the right axis. P48 data in Mould-R filter (filled circles), and P60 data in r-band (open circles) are calibrated using r-band magnitudes of SDSS stars, and expressed in the AB system. For P48, we also include color term corrections estimated considering the $r - i$ SDSS colors of the reference stars. Synthetic photometry obtained from Gemini (filled square) and Keck (filled triangle) spectra is referred to SDSS r-band and expressed in AB system. From the Gemini spectrum, we estimate $R - r \approx -0.1$ mag for the conversion from SDSS r-band magnitudes in AB system, to R-band magnitudes in Vega system. Wise data in the R filter and Vega system (stars), are calibrated to SDSS as described in Jordi et al. (2006). For comparison with P48 photometry, Wise data are shifted to account for $r - R \approx 0.3$ mag for the conversion from SDSS r-band magnitudes in AB system, to Wise R-band magnitudes in Vega system (Jordi et al. 2006). We also plot the R-band light-curve template of SN 1998bw (solid line), SN 2003jd (dotted line), SN 2009bb (dashed line), and SN 2002ap (dash-dotted line), rescaled to the redshift of PTF 10bzf. These templates are obtained interpolating data retrieved from: Galama et al. (1998) for SN 1998bw; Gal-Yam et al. (2002); Foley et al. (2003) for SN 2002ap; Valenti et al. (2008) for SN 2003jd; Pignata et al. (2011) for SN 2009bb.

Table 2—Continued

JD-2455251.004 (days since Feb 23.504)	Telescope	Δt (s)	Band	Mag or Flux	Reference
62.835	P48	60	Mould-R	20.27 ± 0.19	This paper
62.878	P48	60	Mould-R	20.15 ± 0.17	This paper
65.782	P48	60	Mould-R	20.02 ± 0.11	This paper
65.857	P48	60	Mould-R	19.91 ± 0.13	This paper
66.888	P48	60	Mould-R	20.06 ± 0.11	This paper
66.932	P48	60	Mould-R	20.10 ± 0.15	This paper
68.649	P48	60	Mould-R	20.173 ± 0.093	This paper
68.692	P48	60	Mould-R	20.198 ± 0.098	This paper
69.771	P48	60	Mould-R	20.299 ± 0.087	This paper
69.815	P48	60	Mould-R	20.159 ± 0.079	This paper
43.840	P60	180	r	19.47 ± 0.13	This paper
43.841	P60	180	i	19.51 ± 0.32	This paper
44.898	P60	180	z	19.86 ± 0.57	This paper
44.901	P60	180	B	21.63 ± 0.75[a]	This paper
49.960	P60	180	g	21.17 ± 0.17	This paper
49.962	P60	180	r	19.587 ± 0.070	This paper
49.964	P60	180	i	19.746 ± 0.044	This paper
49.965	P60	180	z	18.99 ± 0.31	This paper
49.967	P60	180	B	21.7 ± 1.0[a]	This paper
53.993	P60	180	r	19.72 ± 0.17	This paper
59.895	P60	180	r	19.77 ± 0.20	This paper
65.904	P60	180	i	19.96 ± 0.17	This paper
73.842	P60	180	i	20.15 ± 0.17	This paper
73.844	P60	180	r	20.27 ± 0.17	This paper
78.790	P60	180	r	20.38 ± 0.16	This paper
79.790	P60	180	i	20.50 ± 0.17	This paper
79.794	P60	180	B	21.82 ± 0.83[a]	This paper
79.797	P60	180	g	20.88 ± 0.16	This paper
80.771	P60	180	z	19.47 ± 0.45	This paper
81.848	P60	180	r	20.207 ± 0.084	This paper
99.798	P60	180	i	20.99 ± 0.36	This paper
99.801	P60	180	B	22.5 ± 1.3[a]	This paper

Table 2—Continued

JD-2455251.004 (days since Feb 23.504)	Telescope	Δt (s)	Band	Mag or Flux	Reference
99.803	P60	180	g	21.27 ± 0.19	This paper
102.774	P60	180	r	20.72 ± 0.12	This paper
102.776	P60	180	B	22.45 ± 0.81^a	This paper
102.780	P60	180	g	21.66 ± 0.31	This paper
103.791	P60	180	i	20.80 ± 0.27	This paper
24	Wise (PI)	600	B	20.34 ± 0.57^b	This paper
24	Wise (PI)	600	V	19.08 ± 0.18^b	This paper
24	Wise (PI)	600	R	18.55 ± 0.11^b	This paper
28	Wise (PI)	600	I	18.42 ± 0.20^b	This paper
28	Wise (PI)	600	B	20.60 ± 0.64^b	This paper
28	Wise (PI)	600	V	19.36 ± 0.27^b	This paper
28	Wise (PI)	600	R	18.79 ± 0.20^b	This paper
28	Wise (PI)	600	I	18.60 ± 0.13^b	This paper
35	Wise (LAIWO)	720	V	20.27 ± 0.42^b	This paper
35	Wise (LAIWO)	720	R	18.87 ± 0.14^b	This paper
35	Wise (LAIWO)	720	I	19.00 ± 0.61^b	This paper
38	Wise (LAIWO)	720	V	19.87 ± 0.69^b	This paper
38	Wise (LAIWO)	720	R	19.57 ± 0.34^b	This paper
7	Gemini	450	g^c	18.6 ± 0.3	ATEL 2470
7	Gemini	450	r^c	18.3 ± 0.3	ATEL 2470
7	Gemini	450	i^c	18.7 ± 0.3	ATEL 2470
12	Keck	240	g^c	18.91 ± 0.3	This paper
12	Keck	2×80	r^c	18.48 ± 0.3	This paper
12	Keck	2×80	i^c	18.70 ± 0.3	This paper
8.52	UVOT	5×10^3	B	18.73 ± 0.10	ATEL 2471
8.52	UVOT	5×10^3	U	18.88 ± 0.12	ATEL 2471
8.52	UVOT	5×10^3	$UVW1$	20.07 ± 0.18	ATEL 2471
8.52	UVOT	5×10^3	$UVW2$	20.18 ± 0.26	ATEL 2471
12.80	UVOT	2.5×10^3	U	19.68 ± 0.14	ATEL 2471
12.80	UVOT	2.5×10^3	$UVW1$	20.12 ± 0.24	ATEL 2471
8.52	XRT	5×10^3	$0.3 - 10$ keV	$< 1.3 \times 10^{-14}$ erg s^{-1}cm^{-2}	ATEL 2471
12.80	XRT	2.5×10^3	$0.3 - 10$ keV	$< 2.7 \times 10^{-14}$ erg s^{-1}cm^{-2}	ATEL 2471

2.2. Spectroscopy

Gemini North GMOS[5] (Hook et al. 2004) spectra were taken on 2010 March 2 (Program ID: GN-2010A-Q-20), using a 1″ slit, with the B600 and R400 gratings. The observations had an exposure time of 450 s (see Table 2), the airmass was 1.236, the sky position angle was 191°, and the standard star was Feige34. Standard data reduction was performed with IRAF V2.14, using the Gemini 1.10 reduction packages. The Gemini spectrum of PTF 10bzf is shown in Figure 3. A redshift of $z = 0.0498 \pm 0.0003$ was derived from the host galaxy emission lines of O III, Hα, Hβ, N II, and S II. The spectrum (black line in Figure 3), resembles that of SN 1998bw at a similar epoch (red line in Figure 3 and Galama et al. 1998), and shows very broad lines, leading us to classify this SN as a broad-line Ic.

PTF 10bzf was also observed by Keck I/LRIS[6] using a 1″ slit, with the 400/8500 grating plus 7847 Å central wavelength on the red side, and with the 400/3400 grism on the blue side. The exposure time was $2 \times 80\,\mathrm{s}$ on the red side, and $1 \times 240\,\mathrm{s}$ on the blue side (see Table 2). Keck data were reduced using the standard longslit reduction packages developed in the IRAF environment (Figure 4).

Both Gemini and Keck spectra were used to derive synthetic photometry in SDSS r-, g-, and i-bands (Table 2). Synthetic photometry was performed as described in Poznanski et al. (2002).

2.3. *Swift* follow-up observations

A two-epoch observation of PTF 10bzf was performed as part of a *Swift* Target of Opportunity program[7]. *Swift*/XRT did not detect any X-ray counterpart to PTF 10bzf (Kasliwal & Cenko 2010). The corresponding upper limits are reported in Table 2, where we have converted the 0.3–10 keV XRT count rates into fluxes assuming a photon index of $\Gamma = 2$, and correcting for Galactic absorption ($N_H \approx 10^{20}\,\mathrm{cm}^{-2}$).

During the first epoch, PTF 10bzf was detected by *Swift*/UVOT (Kasliwal & Cenko 2010), and was observed to fade in the subsequent observation. The measured magnitudes in *Swift*/UVOT filters are reported in Table 2.

---

[5]The Gemini Observatory is operated by the Association of Universities for Research in Astronomy, Inc., under a cooperative agreement with the NSF on behalf of the Gemini partnership: the National Science Foundation (United States), the Science and Technology Facilities Council (United Kingdom), the National Research Council (Canada), CONICYT (Chile), the Australian Research Council (Australia), Ministério da Ciência e Tecnologia (Brazil) and Ministerio de Ciencia, Tecnología e Innovación Productiva (Argentina).

[6]The W.M. Keck Observatory is operated as a scientific partnership among the California Institute of Technology, the University of California and the National Aeronautics and Space Administration. The Observatory was made possible by the generous financial support of the W.M. Keck Foundation.

[7]"Unveiling New Classes of Transients with Palomar Transient Factory", PI S. R. Kulkarni

Table 2—Continued

JD-2455251.004 (days since Feb 23.504)	Telescope	Δt (s)	Band	Mag or Flux	Reference
9.69	CARMA	19.8×10^3	95 GHz	$(-3.7 \pm 1.8) \times 10^3 \, \mu$Jy	ATEL 2473
10.14	Allen	4.8×10^3	3.09 GHz	$< 1.5 \times 10^3 \, \mu$Jy	ATEL 2472
17.69	EVLA	5.76×10^3	4.96 GHz	$< 33 \, \mu$Jy	ATEL 2483
86.71	EVLA	3600	6 GHz	$< 36 \mu$Jy	This paper
276.9	EVLA	7200	4.96 GHz	$< 35 \mu$Jy	This paper
18.24	WSRT	28.8×10^3	4.8 GHz	$< 126 \, \mu$Jy	ATEL 2479

[a]B magnitudes (in Vega system) calibrated to SDSS using the conversions described in Jordi et al. (2006).

[b]$BVRI$ magnitudes (in Vega system) calibrated to SDSS using the conversions described in Jordi et al. (2006).

[c]Synthetic photometry is referred to SDSS g, r, i filters (in AB system). Errors are dominated by flux calibration errors.

Note. — Magnitudes are not corrected for Galactic extinction ($E(B - V) = 0.012$ mag; Schlegel et al. 1998). P48 and P60 observations are calibrated to SDSS (which is estimated to be on the AB system within ± 0.01 mag in the r, i and g bands; within ± 0.02 mag in the z band). P48 errors include (in quadrature) zeropoint calibration errors ($\lesssim 0.01$ mag), color term errors ($\lesssim 0.03$ mag), and aperture correction errors ($\lesssim 0.04$ mag). For P48 detections, positive counts were collected in the subtracted images at the SN position and magnitudes are above the image 3σ limiting magnitude. All upper-limits are at 3σ.
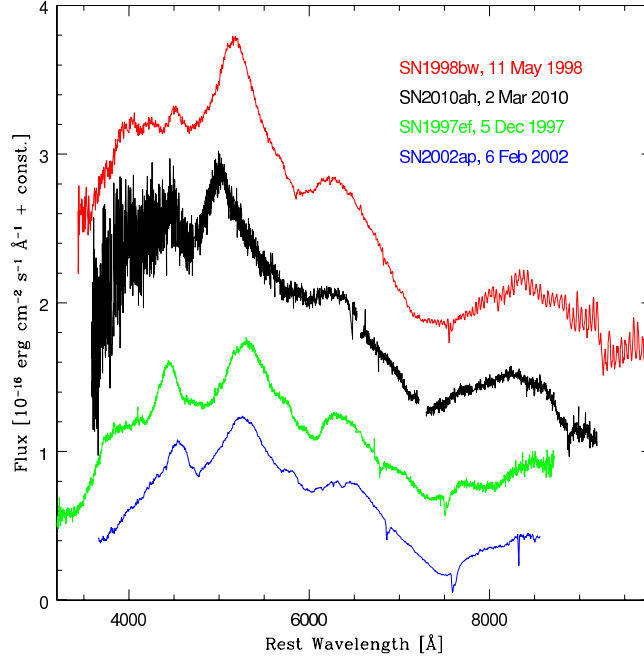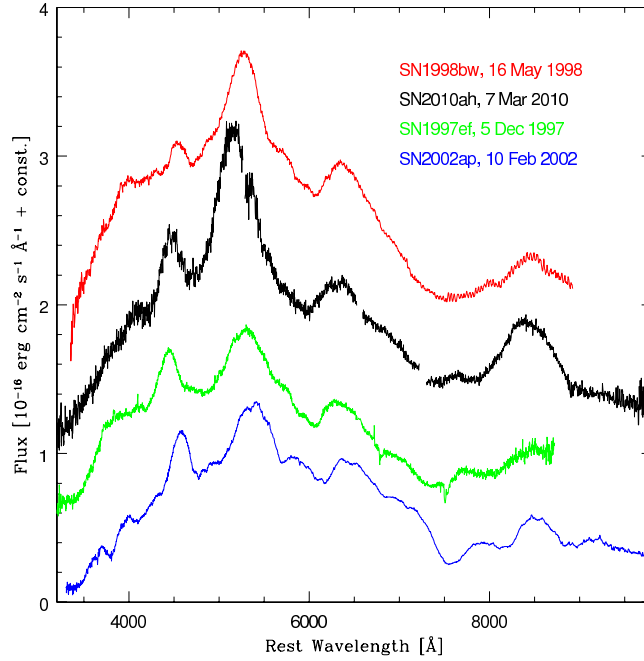
Fig. 3.— Gemini (black) spectrum of PTF 10bzf obtained on 2010 March 2, around the time of the *R*-band maximum. The spectrum is compared with that of SN 1997ef (green), SN 1998bw (red), SN 2002ap (blue) at similar epochs. The SNe are ordered by peak luminosity. This ordering reveals a sequence also in line velocity and blending. The spectrum of SN 1998bw is the most affected by line broadening, as seen for example in the almost complete absence of the re-emission peak near 4500 Å and by the complete blending of the O I 7773 and the Ca II IR triplet. PTF 10bzf is intermediate between SN 1998bw and the two non-GRB SNe 1997ef and 2002ap in both of these respects. Spectral data were retrieved from: Mazzali et al. (2000) for SN 19997ef; Patat et al. (2001) for SN 1998bw; Mazzali et al. (2002) for SN 2002ap. Main telluric lines have been removed from PTF 10bzf spectrum.

Fig. 4.— Keck (black) spectrum of PTF 10bzf obtained on 2010 March 7, about 5 days post *R*-band maximum. The spectrum is compared with that of SN 1997ef (green), SN 1998bw (red), SN 2002ap (blue) at similar epochs. The SNe are ordered by peak luminosity. This ordering reveals a sequence also in line velocity and blending. The spectrum of SN 1998bw is the most affected by line broadening, as seen for example in the almost complete absence of the re-emission peak near 4500 Å and by the complete blending of the O I 7773 and the Ca II IR triplet. PTF 10bzf is intermediate between SN 1998bw and the two non-GRB SNe 1997ef and 2002ap in both of these respects. Spectral data were retrieved from: Mazzali et al. (2000) for SN 19997ef; Patat et al. (2001) for SN 1998bw; Mazzali et al. (2002) for SN 2002ap. Main telluric lines have been removed from PTF 10bzf spectrum.

2.4. Radio follow-up observations

In the radio band, PTF 10bzf was followed-up by the Allen Telescope Array (Welch et al. 2009), by the Combined Array for Research in Millimeter-wave Astronomy (CARMA, Carpenter 2010), and by the Westerbork Synthesis Radio Telescope (WSRT, Kamble et al. 2010). No radio source was detected by any of these telescopes (Table 2).

The Expanded Very Large Array[8] (EVLA; Perley et al. 2009) provided the deepest upper-limit of $33\,\mu$Jy for a radio counterpart associated with PTF 10bzf (Chomiuk & Soderberg 2010, and Table 1).

Starting on 2010 November 27.49, we observed PTF 10bzf with the EVLA in its C configuration, through an EVLA exploratory program (PI: A. Corsi)[9]. We observed for 2 hrs, at a center frequency of 4.96 GHz, and with a total bandwidth of 256 MHz. No radio source was detected at the SN position, the corresponding upper-limit is reported in Table 2. A compact source (J1146+5356) near PTF 10bzf was observed every 6 min for accurate phase calibration, while 3C 286 was observed at the end of the run for the bandpass and flux density calibration. Data were reduced and imaged using the Astronomical Image Processing System (AIPS) software package.

We also reduced with the AIPS archival data that were taken on 2010 May 21.21 (PI: A. Soderberg), for a 1 hr integration time at 6 GHz (with a 1 GHz bandwidth). We find no source at the position of PTF 10bzf, and derive a 3σ upper-limit comparable to the one obtained by Chomiuk & Soderberg (2010) during the first epoch (see Table 2).

3. Comparison with SN 1998bw and GRB search

3.1. Optical emission

Our photometric monitoring program missed the photometric maximum. However, by performing synthetic photometry on the Gemini spectrum taken on 2010 March 2 (about a week after the discovery), and the Keck spectrum taken on 2010 March 7 (about 12 days after the discovery), we derive *g-r-i* magnitudes of PTF 10bzf at these epochs (see Table 2). As evident from Figure 2, PTF 10bzf was likely around maximum light during the Gemini observation. The *R*-band apparent magnitude of PTF 10bzf, as derived from the synthetic photometry on the Gemini spectrum, is $R = 18.4 \pm 0.3$ (AB system, or $R = 18.2 \pm 0.3$ in the Vega system). This gives us an approximate estimate of the SN absolute magnitude around R-band peak time, of $M_R = -18.3 \pm 0.3$ (AB system, or $M_R = -18.5 \pm 0.3$ in the Vega system).

In Figure 2 and Table 1 we summarize the properties of the spectroscopically confirmed broad-line Ic SNe associated with GRBs; of the broad-line Ic SNe 2003jd and 2002ap, as examples of "normal" broad-

---

[8]http://www.aoc.nrao.edu/evla/; The Very Large Array is operated by the National Radio Astronomy Observatory (NRAO), a facility of the National Science Foundation operated under cooperative agreement by Associated Universities, Inc.

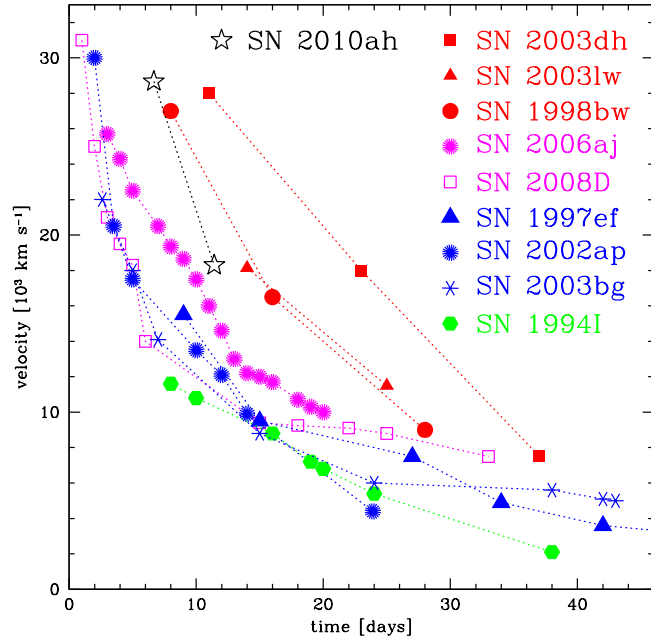[9]VLA/10C-227 - "Late time follow-up of Ic SN PTF 10bzf".

Fig. 5.— The measured Si II line velocity of PTF 10bzf (black stars) compared to photospheric veloc-ities *derived from spectroscopic modeling* for a number of SNe Ib/c. Red symbols represent GRB-SNe (i.e. SN 1998bw, SN 2003dh, SN 2003lw, see Iwamoto et al. 1998; Mazzali et al. 2003, 2006b); magenta is used for XRF/X-ray transients-SNe (i.e. SN 2006aj and SN 2008D, Mazzali et al. 2006a; Pian et al. 2006; Modjaz et al. 2009); blue represent BL-SNe type Ic (SN 1997ef and SN 2002ap Mazzali et al. 2000, 2002) or IIb (SN 2003bg, Mazzali et al. 2009); finally green is used for the "normal" SN Ic 1994I (Sauer et al. 2006).

line Ics; and finally of the broad-line Ic SN 2009bb (Pignata et al. 2011; Soderberg et al. 2010), as prototype of engine-driven SNe with no clear GRB association.

SNe 1998bw (Iwamoto et al. 1998), 2003dh (Mazzali et al. 2003), and 2003lw (Mazzali et al. 2007), all of which produced GRBs, were brighter and more energetic than other broad-line Ic SNe for which a high-energy signal was either not detected (e.g. SNe 1997ef and SN 2002ap, see Mazzali et al. 2000, 2002), or was an XRF (SN 2006aj, Mazzali et al. 2006b). As evident from Table 1 and Figure 2, PTF 10bzf was more luminous than the broad-line Ic SN 2002ap (with a difference in R-band absolute magnitude at peak of $M_{R;10bzf} - M_{R,2002ap} = -1.0 \pm 0.4$); comparable (within the errors) to the engine driven SN 2009bb and to the broad-line Ic SN 2003j around maximum R-band light; less luminous than the GRB-associated SN 1998bw ($M_{R,10bzf} - M_{R,1998bw} = 0.9 \pm 0.3$ at R-band maximum light).

Although the peak epoch is not well known, we can estimate the ^{56}Ni mass in PTF 10bzf by interpolating between the R-band light-curves of SN 2002ap (for which $M_{56Ni} \approx 0.09$ M$_\odot$, Mazzali et al. 2002) and SN 1998bw (for which $M_{56Ni} \approx 0.5$ M$_\odot$, Nakamura 1999; Nakamura et al. 2001). We find that for PTF 10bzf $M_{56Ni} \approx 0.20 - 0.25$ M$_\odot$. The ^{56}Ni mass can also be estimated using the empirical relation derived by Drout et al. (2010) from the properties of a large sample of Ic SNe (including broad-line and engine driven SNe):

$$log(M_{56Ni}/M_\odot) \simeq -0.41 \times M_R - 8.3 \tag{1}$$

where M_{56Ni} is the mass of ^{56}Ni estimated using the formalism of Valenti et al. (2008) (see also Arnett 1982), and M_R is the extinction corrected peak magnitude in the R-band (see also Perets et al. 2010). For PTF 10bzf, using Equation (1), we get $M_{56Ni} \approx 0.2$ $M_\odot$, compatible with what obtained by interpolation. This is comparable to SN 2002aj, associated with XRF 060218 (Mazzali et al. 2006b), and significantly less than all other GRB-associated SNe (see Table 1).

Estimating the kinetic energy requires modeling. However, we can use line velocity as a proxy for it. In Figure 3 and Figure 4 we show a spectroscopic sequence of broad-line Ic SNe, from 2002ap to 1998bw. The first (Figure 3) shows spectra near maximum light, the second (Figure 4) shows spectra obtained about 5 days after maximum. In addition, we show the only near-peak spectrum available of SN 1997ef, a broad-line SN without a GRB (Mazzali et al. 2000). We have ordered the SNe by peak luminosity. This ordering however reveals a sequence also in line velocity and blending. The spectra of SN 1998bw are the most affected by line broadening, as seen for example in the almost complete absence of the re-emission peak near 4500 Å and by the complete blending of the O I 7773 and the Ca II IR triplet. PTF 10bzf is intermediate between SN 1998bw and the two non-GRB SNe 1997ef and 2002ap in both of these respects.

We have measured the velocity of the Si II 6355 Å absorption, which traces reasonably closely the position of the photosphere, in the two available spectra of PTF 10bzf (see Figure 3 and Figure 4). The results are shown in Figure 5, where they are compared to the photospheric velocity of a number of Ib/c SNe, with and without a GRB or an XRF. PTF 10bzf appears to be intermediate in velocity between the GRB-associated SNe (in red) and the non-GRB ones, both broad-lined (blue) and narrow-lined (green). Note that, typically, the measured Si II line velocity is somewhat larger than the photospheric velocity, so the photospheric velocity of PTF 10bzf is likely lower than the values shown in Figure 5. This makes

PTF 10bzf more similar to non GRB-associated SNe.

We can use this line velocity measurement, together with an estimate of the width of the light curve of PTF 10bzf, to derive an approximate estimate of the kinetic energy and ejecta mass for PTF 10bzf. As evident from Figure 2, the light curve of PTF 10bzf has to be stretched in time by a factor of ≈ 1.12 to match the shape of SN 1998bw light curve. Moreover, as evident from Figure 5, the velocity of PTF 10bzf may be a factor of ≈ 0.9 smaller than SN 1998bw. Using the formula for the light curve width as a function of ejecta mass and kinetic energy, as delineated by Arnett (1982), we obtain for PTF 10bzf: $M = (7 \pm 2) \, M_\odot$ and $E_K = (17 \pm 5) \times 10^{51}$ erg.

PTF 10bzf thus appears to have an E_K/M ratio of ≈ 2.5. This is larger than non-GRB SNe like 1997ef (which had $E_K/M \approx 2$) or 2002ap (for which $E_K/M \approx 1.25$), but smaller than SN 1998bw ($E_K/M \approx 3$). We thus conclude that PTF 10bzf probably lacks the mass and energy required to initiate a GRB.

3.2. X-ray upper limit

The *Swift*/XRT upper limit for PTF 10bzf at 8.5 days, constrains any X-ray source associated with PTF 10bzf to have a flux $< 1.3 \times 10^{-14}$ erg s^{-1}cm^{-2}, which at the redshift of PTF 10bzf corresponds to an isotropic luminosity of $< 7.4 \times 10^{40}$ erg s^{-1}.

The X-ray flux of GRB 980425 about 1 day after the burst was $\approx 3 \times 10^{-13}$ erg s^{-1}cm^{-2}, and it declined at a rate of $\propto t^{-0.2}$ (Nakamura 1999; Pian et al. 2000). Rescaling it at 8.5 days and taking into account SN 1998bw distance, we obtain an X-ray isotropic luminosity of $\approx 3 \times 10^{40}$ erg s^{-1}, a factor of ≈ 2.5 below our X-ray luminosity upper-limit on PTF 10bzf.

For GRB 030329, an X-ray flux upper-limit of $< 2.6 \times 10^{-12}$ erg s^{-1}cm^{-2} was set at an epoch of about 8 days since the burst, using Rossi-XTE observations (Tiengo et al. 2003). From broad-band afterglow modeling, the predicted X-ray flux at 8 days was $\approx 4 \times 10^{-13}$ erg s^{-1}cm^{-2} (see Figure 4 in Tiengo et al. 2003), which at the redshift of GRB 030329 corresponds to an isotropic luminosity of $\approx 3 \times 10^{43}$ erg s^{-1}, a factor of ≈ 400 higher than our upper-limit on PTF 10bzf.

GRB 031203 had an estimated X-ray flux of $\approx 10^{-13}$ erg s^{-1}cm^{-2} around 8 days (derived extrapolating from the XMM-Newton observations, see Figure 1 in Watson et al. 2004). This corresponds to an isotropic X-ray luminosity of $\approx 3 \times 10^{42}$ erg s^{-1}, a factor of ≈ 40 higher than our X-ray luminosity upper-limit on PTF 10bzf.

For GRB/XRF 060218, *Swift*/XRT measured a flux of $\approx 1.3 \times 10^{-13}$ erg s^{-1}cm^{-2} around 8 days since trigger (see the upper-panel of Figure 2 in Campana et al. 2006). This gives an isotropic X-ray luminosity of $\approx 3 \times 10^{41}$ erg s^{-1}, a factor of ≈ 4 above PTF 10bzf upper-limit.

Finally, *Swift*/XRT observations set an upper-limit of $\approx 3 \times 10^{-14}$ erg s^{-1}cm^{-2} on GRB 100316D X-ray flux around 8 days since the burst (see Figure 6 in Starling et al. 2010), i.e. an isotropic luminosity upper-limit of $\approx 2 \times 10^{41}$ erg s^{-1}, a factor of ≈ 3 greater than our upper-limit on PTF 10bzf.

In conclusion, at ≈ 8 days since trigger, all GRBs with a spectroscopically confirmed associated SN, had an X-ray isotropic luminosity larger than our upper-limit on PTF 10bzf, except for GRB 980425.

3.3.   Early time ($t \lesssim 20$ days) radio upper-limits

The novelty of SN 1998bw was in the discovery of prompt radio emission just a few days after GRB 980425 (Kulkarni et al. 1998). The brightness temperature suggested that the radio photosphere moved relativistically ($\Gamma \geq 2$), with a total energy of $\approx 10^{50}$ erg (Li & Chevalier 1999), about two orders of magnitude less than the total kinetic energy of the explosion, which was estimated to be of $\approx 3 \times 10^{52}$ erg (Iwamoto et al. 1998). None of these last features, together with the spatial and temporal association with a GRB, were ever observed for a nearby SN before SN 1998bw, thus suggesting the presence of a central engine powering this explosion.

SN 2003dh, associated with GRB 030329, showed an isotropic energy of $\approx 4 \times 10^{52}$ erg, which leaded to classify this event as an "hypernova" (Mazzali et al. 2003). The radio afterglow of GRB 030329 was $\gtrsim 100$ times more luminous than SN 1998bw (Berger et al. 2003a). Berger et al. (2003a) modeled such emission as due to the contribution of a second jet component, wider than the one generating the burst itself, and having an isotropic kinetic energy of $\approx 5.6 \times 10^{51}$ erg.

SN 2003lw, associated with GRB 031203, had a total kinetic energy of $\approx 6 \times 10^{52}$ ergs (Mazzali et al. 2006b). The spectral peak luminosity in radio was $\approx 10^{29}$ erg s^{-1} Hz^{-1}, about a factor of 100 less luminous than the radio afterglow of GRB 030329, but comparable to the radio peak luminosity of SN 1998bw. The kinetic energy in the afterglow component giving rise to the radio emission was estimated to be of $\approx 1.7 \times 10^{49}$ erg (Soderberg et al. 2004).

The total kinetic energy of SN 2006aj was $\approx 2 \times 10^{51}$ erg (Mazzali et al. 2006a), smaller than the other GRB-associated SN. The radio afterglow of XRF 060218 peaked at about 5 days since the trigger, the peak luminosity being about a factor of 10 less bright than SN 1998bw at peak (Soderberg et al. 2006b). The kinetic energy and Lorentz factor around the time of the radio peak were estimated to be of $\approx 2 \times 10^{48}$ erg and $\Gamma \approx 2.3$, respectively (Soderberg et al. 2006b).

SN 2010bh, the latest spectroscopically confirmed SN associated with a GRB, had a kinetic energy of $\approx 1.39 \times 10^{52}$ erg (Cano et al. 2011). Radio upper-limits at about 2 days since the burst constrain the radio spectral luminosity to be below 8×10^{27} erg s^{-1} Hz^{-1}, a factor of 2-to-10 lower than the radio afterglow luminosities observed for SN 1998bw, GRB 031203, and XRF 060218 on comparable timescales (Wieringa et al. 2010).

At a redshift of $z = 0.0498$, the deepest early time radio upper-limit for PTF 10bzf was obtained by Chomiuk & Soderberg (2010). This sets a limit of on the spectral luminosity of $L_{5\,\text{GHz}} < 1.6 \times 10^{27}$ erg s^{-1} Hz^{-1}, at about three weeks after the explosion. This is ≈ 20 times lower than the radio luminosity observed on a similar timescale for the Ic SN 1998bw and SN 2009bb (Soderberg et al. 2010), the only two SNe which showed clear evidence for energetic and mildly-relativistic outflows (Chomiuk & Soderberg 2010). How-
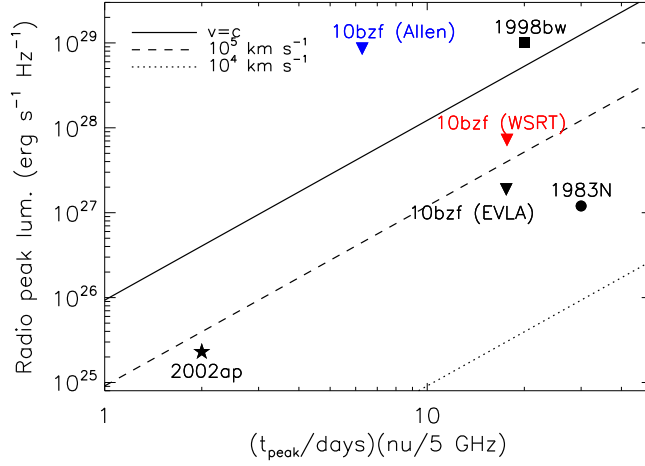
Fig. 6.— Constraints on approximate expansion velocity derived from the early-time Allen telescope (blue triangle), WSRT (red triangle), and EVLA (black triangle) radio upper-limits on PTF 10bzf (see Table 2 and Equation 2), compared with similar constraints obtained from the radio detections of SN 1998bw (black square), SN 1983N (black dot), and SN 2002ap (black star) (see Figure 2 in Berger et al. 2003b, for comparison). As evident, SN 1998bw with $v_r \sim c$ remains an exception. The Allen upper-limit on PTF 10bzf around its peak time ($\sim$ 10 days since discovery, see Table 2) does not exclude a relativistic expansion. However, $v \sim c$ is indeed excluded by the radio upper-limits obtained about a week later by EVLA and WSRT. We stress that while the upper limits do not necessarily measure the peak of the spectrum at the time of the observation, typically time delays of few tens of days relative to the SN explosion reasonably sample the peak. However, if PTF10bzf peaked at few days after the explosion like SN 2002ap, the EVLA and WSRT upper-limits would not be deep enough to rule out a relativistic expansion.

ever, we note that this upper-limit is comparable to the radio luminosity of GRB 060218 at a similar epoch (Soderberg et al. 2006b).

Using the early-time radio upper-limit, we constrain the mean expansion speed v_r of the radio photosphere. Under the reasonable assumption that radio emission arises from a synchrotron spectrum with $\nu_a \sim \nu_p$ (where ν_a is the self-absorption frequency and ν_p the peak frequency), and under the hypothesis of equipartition, the peak-time t_p and peak-luminosity L_p of the radio emission directly measure the average expansion speed (Berger et al. 2003b; Chevalier 1998; Kulkarni et al. 1998; Scott & Readhead 1977):

$$ v_r \sim 3.1 \times 10^4 \left(\frac{L_p}{10^{26} \text{erg s}^{-1}} \right)^{17/36} \left(\frac{t_p}{10 \text{ days}} \right)^{-1} \left(\frac{\nu_p}{5 \text{ GHz}} \right)^{-1} \text{ km s}^{-1} . \tag{2} $$

Figure 6 shows $L_{5\,\text{GHz}}$ at peak versus $t_p \nu_p$ for different values of v_r, compared with the Allen telescope, WSRT and EVLA upper-limits on PTF 10bzf. Assuming that the radio emission peaked at ≈ 18 days, the WSRT and EVLA observations constrain the expansion velocity to be less than 10^5 km s^{-1}.

Estimating the expansion velocities for non-detections has the caveat that the radio peak epoch is in reality unknown. However, as noted by Berger et al. (2003b), observations performed at $\sim 10 - 20$ days since explosion, sample the radio peak time of Ic SN reasonably well. E.g. SN 1983N peaked in radio at ~ 30 days after explosion, while the radio light-curve of SN 1998bw showed a double-peak profile, with the first peak around 10 days since explosion, and the second around 30 days after explosion. This justifies our use of radio upper-limits taken within ≈ 3 weeks since discovery to constrain the expansion speed. We also note, however, that if PTF10bzf peaked at few days after the explosion like SN 2002ap, the EVLA and WSRT upper-limits would not be deep enough to rule out a relativistic expansion.

3.4. Late time ($t \gtrsim 20$ days) radio upper-limits

In the context of the fireball model, the emission from an off-axis GRB is expected to be visible in the radio band long past the GRB explosion (at timescales of the order of ~ 1 yr, see Levinson et al. 2002). In fact, at sufficiently late times, the relativistic fireball is expected to enter the sub-relativistic phase, during which the jet starts spreading, rapidly intersecting the viewer's line of sight as the ejecta approaches spherical symmetry.

To model the late-time radio emission from an off-axis GRB during the non-relativistic phase, we use the analytical model by Waxman (2004b) for a fireball expanding in a wind medium (see e.g. Levinson et al. 2002, for the constant ISM case). In this model the radio luminosity is approximated as (see also Perna & Loeb 1998; Livio & Waxman 2000; Paczynski 2001; Granot et al. 2002; Berger et al. 2003b; Soderberg et al. 2006a; van Eerten et al. 2010):

$$ L_r \sim 2.1 \times 10^{29} \left(\frac{\epsilon_e \epsilon_B}{0.01} \right)^{3/4} \left(\frac{\nu}{10 \text{ GHz}} \right)^{-\frac{(p-1)}{2}} \left(\frac{t}{t_{NR}} \right)^{-3/2} $$
$$ \times A_*^{9/4} E_{51}^{-1/2} \text{ erg s}^{-1} \text{ Hz}^{-1}, \tag{3} $$

where E_{51} is the beaming-corrected ejecta energy, A_* defines the circumstellar density in terms of the pro-
genitor mass loss-rate $\dot{M}$ and wind velocity v_w such that $\dot{M}/4\pi v_w = 5 \times 10^{11} A_* \, \mathrm{g\,cm^{-1}}$ (Waxman 2004b;
Soderberg et al. 2006a), and:

$$t_{NR} \sim 0.3 \left(\frac{E_{51}}{A_*} \right) \mathrm{yr}, \tag{4}$$

is the time of the non-relativistic transition. Note that in the above formulation it is assumed that the fireball
spreads sideways at approximately the speed of light. By imposing $t_{NR} \lesssim t_{obs}$ and $L_r \gtrsim L_{obs}$, we can use
the EVLA observations of PTF 10bzf (see Table 2) to exclude the values of (beaming corrected) energy
and wind density that would give a radio luminosity above the upper-limits of PTF 10bzf, at the times of
our observations. The exclusion regions obtained in this way are plotted in yellow in Figure 7. We can
compare these constraints with the energy and density derived from the broad-band afterglow modeling of
GRB 980425, GRB 030329 and GRB 031203 (see Soderberg et al. 2006a; Waxman 2004a, and references
therein), also plotted in Figure 7. From such a comparison we conclude that a GRB fireball possibly as-
sociated with PTF 10bzf, could not have the same (beaming corrected) energy and wind density of GRB
030329 and GRB 031203. In fact, if this was the case, such a fireball would have been in its non-relativistic
(spherical) phase at the times of our radio observations (so that its radio emission would be observable by
any off-axis observer), and its radio luminosity would be greater than our upper-limits for PTF 10bzf.

We stress that our Figure 7 only constrains the portion of the parameter space where $t_{NR} \lesssim t_{obs}$. This
provides an estimate of the values of the fireball parameters ruled out by our observations, which does not
depend critically on the adopted model. Constraining the portion of the parameter space where $t_{NR} \gtrsim t_{obs}$,
requires detailed modeling. In fact, before t_{NR}, the sideways expansion and the deceleration of the jet depend
on the spatial distribution within the jet of the energy density and the Lorentz factor. These distributions
are poorly constrained by current observations. And, for given distributions, an accurate calculation of jet
expansion and deceleration requires to be carried out numerically.

3.5. Search for γ-rays

We searched for a possible GRB in coincidence with PTF 10bzf using the IPN data. We searched for
bursts with a localization error-box including PTF 10bzf. Since the exact explosion epoch of PTF 10bzf
is not known, we searched in a time-window, extending from 2010 February 12 to 2010 February 23 (the
discovery day of PTF 10bzf). We conservatively extend such a time window to include one full week prior to
our last non-detection of PTF 10bzf. Therefore, our time window starts ≈ 11 days before the SN discovery
(i.e. ≈ 18 days before its R-band maximum light).

For comparison, we note that the engine driven SN 2009bb reached its maximum light about two weeks
after the estimated explosion date (Soderberg et al. 2010), evolving somewhat faster than SN 1998bw in the
pre-peak phase (Pignata et al. 2011). As evident from Figure 2, our last upper-limit on 2010 February 19
($R > 21.3$) indicates that also PTF 10bzf probably evolved more rapidly than SN 1998bw in its pre-peak
phase. Using the R-band light curve as a proxy for $L(t)$, and assuming a pre-peak luminosity evolution
$L(t) \propto (t - t_0)^{1.8}$ (where t_0 is the explosion time, see e.g. Pignata et al. 2011), t_0 should be in between $\approx$

2010 February 17.80 and $\approx$ 2010 February 23.50 (i.e. PTF discovery date) to account for the $\gtrsim$ 2.44 mag drop observed between our last non-detection of PTF 10bzf, and its discovery. However, we conservatively extend our time interval for the GRB search to 2010 February 12, one week prior to our last non-detection (on 2010 February 19.443).

Between 2010 February 12 and 2010 February 23, a total of 14 confirmed bursts were detected by the spacecrafts of the interplanetary network (IPN[10]: Mars Odyssey, Konus-Wind, RHESSI, INTEGRAL (SPI-ACS), *Swift*-BAT, MESSENGER, Suzaku, AGILE, and *Fermi* (GBM)). Here confirmed means that they were observed by more than one detector on one or more spacecraft, and could be localized at least coarsely.

The localization accuracies of these 14 bursts varied widely, but none of them was found to be consistent with the position of PTF 10bzf. One burst was observed by the *Fermi* GBM alone (error circles with 1σ statistical-only error radii of 10.5 degrees), while other five were observed by the GBM and other spacecrafts. Four events were observed by a distant IPN spacecraft, and could be triangulated to annuli or error boxes with dimensions as small as $\sim 10'$. Five GRBs were observed within the coded field of view of the *Swift* BAT ($3'$ initial localization accuracy), and in some cases by other IPN spacecrafts as well.

PTF 10bzf is not spatially associated with any of these GRBs. The total area of the localizations of the 14 confirmed bursts, containing the 3σ error regions, was ≈ 1.3 *sr*. Therefore, there is only $\approx 10\%$ chance coincidence between these bursts and PTF 10bzf.

Next, based on our GRB sample, we can put a limit on the fluence of any GRB associated with PTF 10bzf. We considered three distinct sets of events: IPN bursts, *Fermi* GBM-only bursts, and *Swift* BAT-only bursts. The IPN is sensitive to bursts with fluences down to about 6×10^{-7} erg cm^{-2} (50% efficiency - see Hurley et al. 2010), and observes the entire sky with a temporal duty cycle close to 100%. The *Fermi* GBM detects bursts down to a $8 - 1000$ keV fluence of about 4×10^{-8} erg cm^{-2}, and observes the entire unocculted sky (≈ 8.8 sr) with a temporal duty cycle of more than 80%. The weakest burst observed by the BAT had a 15-150 keV fluence of 6×10^{-9} erg cm^{-2}, and the BAT observes a field of view of about 2 sr with a temporal duty cycle of about 90%.

If the SN produced a burst below the IPN threshold, and above the *Fermi* one, it is possible that both *Swift* and *Fermi* did not detect it: considering their spatial and temporal coverages, the non-detection probabilities are about 0.86 and 0.44, respectively. Finally, if the SN produced a burst below the *Fermi* threshold, but above the *Swift* one, the non-detection probability is about 0.86. We note that a burst with an isotropic energy release comparable to that of the sub-energetic GRB 980425, $E_{\rm iso} \approx 6 \times 10^{47}$ ergs, placed at the distance of PTF 10bzf, would be observed with a fluence of $\approx 10^{-7}$ erg cm^{-2}, which is below the IPN threshold, but above the *Fermi* GBM one.

---

[10]http://www.ssl.berkeley.edu/ipn3/

4. Conclusion

We presented the discovery of PTF 10bzf, a broad-line type Ic SN detected by PTF. We obtained multi-wavelength follow-up observations of this SN, we compared its properties with those of other SNe associated with GRBs, and put limits on any associated GRB using the IPN sample.

While PTF 10bzf shows some spectral similarities with SN 1998bw, its R-band and radio luminosities are much lower, with no clear evidence for a relativistic expansion speed. The spectral properties of PTF 10bzf suggest that this SN is intermediate, in terms of explosion kinetic energy, between non-GRB associated SNe like 2002ap or 1997ef, and GRB-associated SNe like 1998bw. A search for γ-rays using the IPN sample, gives no GRB with a position consistent with this SN, in a time-window extending to a full week prior to our last non-detection of the source. We thus conclude that PTF 10bzf probably lacks the mass and energy required to initiate a GRB.

Despite the fact that PTF 10bzf does not show evidence for being associated with a nearby GRB, the discovery and follow-up of broad-line Ic SNe remains a fundamental tool to investigate the GRB-SN connection. Broad-line Ic SNe are rare, and they are the only type of SNe which have confirmed associations with GRBs. Therefore, it is crucial to study them, and determine how the GRB-associated SNe differ from the other broad-line Ic SN. PTF is a project able to discover and classify about ten broad-line Ic SNe per year, thus allowing to construct a large sample of SNe which are unique broad-line Ic.

The search for SNe associated with nearby (non γ-ray triggered) GRBs, is particularly relevant also in the light of multi-messenger astronomy. In an era in which ground-based gravitational wave detectors like LIGO[11] and Virgo[12] are approaching their advanced configurations, nearby GRBs represent promising candidates for the detection of gravity waves (e.g. Kobayashi & Mészáros 2003; Kokkotas 2004; Woosley & Bloom 2006; Piro & Pfahl 2007; Corsi & Mészáros 2009; Ott 2009, and references therein). The simultaneous operation of facilities like PTF and LIGO may open, in the forthcoming years, a unique opportunity for this kind of multi-messenger searches (e.g. Bloom et al. 2009; Smith et al. 2009; Stamatikos et al. 2009; Shawhan et al. 2010, and references therein).

---

[11]www.ligo.org

[12]www.virgo.infn.it

REFERENCES

Abdo, A. A., et al. 2009a, Nature, 462, 331

—. 2009b, ApJL, 706, L138

—. 2009c, Science, 323, 1688

Arcavi, I., et al. 2010, ApJ, 721, 777

Arnett, W. D. 1982, ApJ, 253, 785

Balberg, S., & Loeb, A. 2011, MNRAS, 478, 1715

Berger, E., et al. 2003a, Nature, 426, 154

—. 2003b, ApJ, 599, 408

Bersier, D., et al. 2004, GRB Coordinates Network, 2544, 1

Bloom, J. S., Frail, D. A., & Kulkarni, S. R. 2003, ApJ, 594, 674

Bloom, J. S., et al. 2009, ArXiv e-prints 0902.1527

Bucciantini, N., et al. 2008, MNRAS, 383, L25

Bufano, F., et al. 2010, Central Bureau Electronic Telegrams, 2227, 1

Campana, S., et al. 2006, Nature, 442, 1008

Cano, Z., et al. 2011, ArXiv e-prints 1104.5141

Carpenter, J. M. 2010, The Astronomer's Telegram, 2473, 1

Chevalier, R. A. 1976, ApJ, 207, 872

—. 1992, ApJ, 394, 599

—. 1998, ApJ, 499, 810

Chevalier, R. A., & Fransson, C. 2008, ApJL, 683, L135

Chomiuk, L., & Soderberg, A. 2010, The Astronomer's Telegram, 2483, 1

Chornock, R., et al. 2010, ArXiv e-prints, 1004.2262

Cobb, B. E., et al. 2004, ApJL, 608, L93

Corsi, A., Guetta, D., & Piro, L. 2010, ApJ, 720, 1008

Corsi, A., & Mészáros, P. 2009, ApJ, 702, 1171

Della Valle, M., et al. 2006, Nature, 444, 1050

Deng, J., et al. 2005, ApJ, 624, 898

Drout, M. R., et al. 2010, ArXiv 1011.4959

Ferrero, P., et al. 2006, A&A, 457, 857

Filippenko, A. V. 1997, ARA&A, 35, 309

Foley, R. J., et al. 2003, PASP, 115, 1220

Frail, D. A., et al. 2001, ApJL, 562, L55

Fruchter, A. S., et al. 2006, Nature, 441, 463

Fynbo, J. P. U., et al. 2003, A&A, 406, L63

—. 2006, Nature, 444, 1047

Gal-Yam, A., Maoz, D., Guhathakurta, P., & Filippenko, A. V. 2008, ApJ, 680, 550

Gal-Yam, A., Ofek, E. O., & Shemmer, O. 2002, MNRAS, 332, L73

Gal-Yam, A., et al. 2004, ApJL, 609, L59

—. 2006a, Nature, 444, 1053

—. 2006b, ApJ, 639, 331

Galama, T. J., et al. 1998, Nature, 395, 670

Garnavich, P., et al. 2003, IAU Circ., 8114, 1

Gezari, S., et al. 2008, ApJL, 683, L131

Granot, J., Panaitescu, A., Kumar, P., & Woosley, S. E. 2002, ApJL, 570, L61

Grassberg, E. K., Imshennik, V. S., & Nadyozhin, D. K. 1971, APSS, 10, 28

Guetta, D., & Della Valle, M. 2007, ApJL, 657, L73

Hjorth, J., et al. 2003, Nature, 423, 847

Hook, I. M., et al. 2004, PASP, 116, 425

Hurley, K., et al. 2010, in Italian Phys. Soc. Conf. Proc., ed. Eds. G. Chincarini, P. D'Avanzo, R. Margutti, and R. Salvaterra, Vol. 102, 529

Iwamoto, K., et al. 1998, Nature, 395, 672

Jordi, K., Grebel, E. K., & Ammon, K. 2006, A&A, 460, 339

Kamble, A. P., et al. 2010, The Astronomer's Telegram, 2479, 1

Kasliwal, M. M., & Cenko, S. B. 2010, The Astronomer's Telegram, 2471, 1

Katz, B., Budnik, R., & Waxman, E. 2010, ApJ, 716, 781

Katz, B., Sapir, N., & Waxman, E. 2011, ArXiv e-prints, 1103.5276

Kawabata, K. S., et al. 2003, ApJL, 593, L19

Kobayashi, S., & Mészáros, P. 2003, ApJ, 589, 861

Kokkotas, K. D. 2004, Classical and Quantum Gravity, 21, 501

Kulkarni, S. R., et al. 1998, Nature, 395, 663

Law, N. M., et al. 2009, PASP, 121, 1395

Levinson, A., et al. 2002, ApJ, 576, 923

Li, Z., & Chevalier, R. A. 1999, ApJ, 526, 716

Liang, E., Zhang, B., Virgili, F., & Dai, Z. G. 2007, ApJ, 662, 1111

Liang, E.-W., et al. 2008, ApJ, 675, 528

—. 2010, ApJ, 725, 2209

Lithwick, Y., & Sari, R. 2001, ApJ, 555, 540

Livio, M., & Waxman, E. 2000, ApJ, 538, 187

MacFadyen, A. I., & Woosley, S. E. 1999a, ApJ, 524, 262

—. 1999b, ApJ, 524, 262

Malesani, D., et al. 2004, ApJL, 609, L5

Matheson, T., et al. 2003, ApJ, 599, 394

Mazzali, P. A., Deng, J., Hamuy, M., & Nomoto, K. 2009, ApJ, 703, 1624

Mazzali, P. A., Iwamoto, K., & Nomoto, K. 2000, ApJ, 545, 407

Mazzali, P. A., et al. 2002, ApJL, 572, L61

—. 2003, ApJL, 599, L95

—. 2005, Science, 308, 1284

—. 2006a, Nature, 442, 1018

—. 2006b, ApJ, 645, 1323

—. 2007, ApJ, 670, 592

Mészáros, P. 2006, Reports on Progress in Physics, 69, 2259

Metzger, B. D., et al. 2011, MNRAS, 413, 2031

Modjaz, M., et al. 2006, ApJ, 645, L21

—. 2008, AJ, 135, 1136

—. 2009, ApJ, 702, 226

Nagakura, H., Ito, H., Kiuchi, K., & Yamada, S. 2011, ApJ, 731, 80

Nakamura, T. 1999, ApJL, 522, L101

Nakamura, T., Mazzali, P. A., Nomoto, K., & Iwamoto, K. 2001, ApJ, 550, 991

Nakar, E., & Sari, R. 2010, ApJ, 725, 904

Norris, J. P. 2002, ApJ, 579, 386

Ofek, E. O., et al. 2007, ApJ, 662, 1129

—. 2010a, The Astronomer's Telegram, 2470, 1

—. 2010b, ApJ, 724, 1396

Ott, C. D. 2009, Classical and Quantum Gravity, 26, 204015

Paczynski, B. 2001, Acta Astronomica, 51, 1

Patat, F., et al. 2001, ApJ, 555, 900

Perets, H. B., et al. 2010, Nature, 465, 322

Perley, R., et al. 2009, IEEE Proceedings, 97, 1448

Perna, R., & Loeb, A. 1998, ApJL, 509, L85

Pian, E., et al. 2000, ApJ, 536, 778

—. 2006, Nature, 442, 1011

Pignata, G., et al. 2011, ApJ, 728, 14

Piran, T. 1999, Phys. Rep, 314, 575

—. 2004, Reviews of Modern Physics, 76, 1143

Piro, A. L., & Pfahl, E. 2007, ApJ, 658, 1173

Podsiadlowski, P., et al. 2004, ApJ, 607, L17

Poznanski, D., et al. 2002, PASP, 114, 833

Proga, D., & Begelman, M. C. 2003, ApJ, 592, 767

Rabinak, I., & Waxman, E. 2011, ApJ, 728, 63

Racusin, J. L., et al. 2009, ApJ, 698, 43

Rau, A., et al. 2009, PASP, 121, 1334

Rhoads, J. E. 2003, ApJ, 591, 1097

Sauer, D. N., et al. 2006, MNRAS, 369, 1939

Schawinski, K., et al. 2008, Science, 321, 223

Schlegel, D. J., Finkbeiner, D. P., & Davis, M. 1998, ApJ, 500, 525

Scott, M. A., & Readhead, A. C. S. 1977, MNRAS, 180, 539

Shawhan, P. S., LIGO Scientific Collaboration, & Virgo Collaboration. 2010, in Bulletin of the American Astronomical Society, Vol. 42, American Astronomical Society Meeting Abstracts n. 215, 406.06

Smith, J., et al. 2009, in Bulletin of the AAS, Vol. 41, Bulletin of the American Astronomical Society, 443

Soderberg, A. M., Nakar, E., Berger, E., & Kulkarni, S. R. 2006a, ApJ, 638, 930

Soderberg, A. M., et al. 2004, Nature, 430, 648

—. 2006b, Nature, 442, 1014

—. 2008, Nature, 453, 469

—. 2010, Nature, 463, 513

Sollerman, J., et al. 2006, A&A, 454, 503

Stamatikos, M., et al. 2009, in astro2010: decadal Survey, ArXiv 0902.3022, 284

Stanek, K. Z., et al. 2003, ApJL, 591, L17

Starling, R. L. C., et al. 2010, ArXiv e-prints 1004.2919

Thompson, T. A., Chang, P., & Quataert, E. 2004, ApJ, 611, 380

Tiengo, A., et al. 2003, A&A, 409, 983

Toma, K., Ioka, K., Sakamoto, T., & Nakamura, T. 2007, ApJ, 659, 1420

Usov, V. V. 1992, Nature, 357, 472

Valenti, S., et al. 2008, MNRAS, 383, 1485

van Eerten, H., Zhang, W., & MacFadyen, A. 2010, ApJ, 722, 235

Virgili, F. J., Liang, E., & Zhang, B. 2009, MNRAS, 392, 91

Watson, D., et al. 2004, ApJL, 605, L101

Waxman, E. 2004a, ApJL, 605, L97

—. 2004b, Apj, 602, 886

Waxman, E., Mészáros, P., & Campana, S. 2007, ApJ, 667, 351

Welch, J., et al. 2009, IEEE Proceedings, 97, 1438

Wieringa, M., Soderberg, A., & Edwards, P. 2010, GRB Coordinates Network, Circular Service, 10533, 1 (2010), 533, 1

Wiersema, K., et al. 2010, GRB Coordinates Network, Circular Service, 10525, 1 (2010), 525, 1

Woosley, S. E. 1993, ApJ, 405, 273

Woosley, S. E., & Bloom, J. S. 2006, ARA&A, 44, 507

Woosley, S. E., & Heger, A. 2006, ApJ, 637, 914

Woosley, S. E., & Zhang, W. 2007, Royal Society of London Philosophical Transactions Series A, 365, 1129

Yaron, S. E., et al. 2011, in preparation

York, D. G., et al. 2000, ApJ, 120, 1579

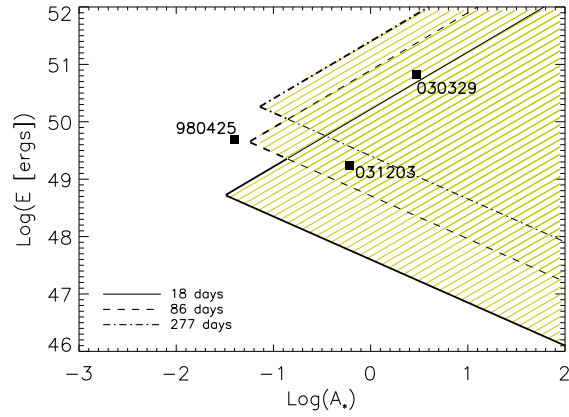Zhang, B., Kobayashi, S., & Mészáros, P. 2003, ApJ, 595, 950

Fig. 7.— Off-axis emission from a GRB explosion associated with PTF 10bzf. The yellow shadowed regions mark the portion of the energy-density plane excluded by the first, second, and third epoch EVLA observations, respectively (see Table 2). As evident from the figure, late-time radio observations are fundamental to exclude the higher energy - higher density region of the energy-density plane. This region contains the most common values of energies and densities ($E_{51} \sim 1 - 10$ and $A_* \sim 1$) observed for long GRBs. We also show for comparison some of the parameters estimated from broad-band modeling of GRBs associated with SNe (980425, 030329, and 031203, see Soderberg et al. 2006a; Waxman 2004a, and references therein).